Self-assembly of model amphiphilic peptides in non-aqueous solvents: changing driving forces, same structure?

Alessandra Del Giudice,*,† Axel Rüter,*,‡ Nicolae Viorel Pavel,† Luciano Galantini,† and Ulf Olsson‡

†*Department of Chemistry, Sapienza University of Rome, P. le A. Moro 5, 00185 Rome, Italy.*

‡*Division of Physical Chemistry, Lund University, SE-22100 Lund, Sweden*

E-mail: alessandra.delguidice@uniroma1.it; axel.rueter@fkem1.lu.se

Abstract

Within the homologous series of amphiphilic peptides A_nK, both A_8K and $A_{10}K$ self-assemble in water to form twisted-ribbon fibrils with lengths around 100 nm. The structure of the fibrils can be described in terms of twisted β-sheets extending in the direction of the fibril, laminated to give a constant cross section of 4 nm by 8 nm. The finite width of the twisted ribbons can be reasonably explained within a simple thermodynamic model, considering a free energy penalty for the stretching of hydrogen bonds along the twisted β-sheets, and an interfacial free energy gain for of the lamination of the hydrophobic β-sheets. In this study, we characterize the self-assembly behavior of these peptides in non-aqueous solutions as a way to probe the role of the hydrophobic interaction in fibril stabilization.

Both peptides, in methanol and N,N-dimethylformamide, were found to form fibrillar aggregates with the same β-sheet structure as in water, but with slightly smaller

cross-section sizes. However, the gel-like texture, the slow relaxation in dynamic light scattering experiments, and a correlation peak in the small angle x-ray scattering pattern highlighted enhanced inter-fibrils interaction in the non-aqueous solvents, in the same concentration range. This could be ascribed to a higher effective volume of the aggregates due to enhanced fibril growth and length, as suggested by light scattering and cryogenic-transmission electron microscopy analysis.

These effects can be discussed considering how the solvent properties affect the different energetic contributions (hydrophobic, electrostatic, hydrogen bonding) to fibril formation. In the analyzed case the decreased hydrogen bonding propensity of the non-aqueous solvents makes the hydrogen bond formation along the fibril a key driving force for peptide assembly, whereas it represents a non-relevant contribution in water.

Introduction

Understanding the driving forces for peptide self-assembly is of both fundamental and practical significance. These aggregation processes are relevant in the formation of protein- and peptide-based amyloid fibrils involved in both diseases and functional aspects of biological systems.[1,2] Peptide self-assembly also represents a versatile tool for building structural elements made of designed peptide building blocks for advanced biomaterials applications.[3–5] In addition, for a growing field such as peptide-based therapeutics, knowing the phase behavior and stability of various peptide solutions and formulations, is of outmost importance.[6] Due to the multifaceted chemical nature of the natural amino acids composing the peptide building blocks, their self-assembly is dictated by various noncovalent interactions (hydrophobic effect, hydrogen bonding, electrostatic interactions, π-π stacking) and their interplay.[7] Their relative importance will depend on the peptide sequence as well as the properties of the surroundings, determining a complex free energy landscape with deep valleys corresponding to low free energy states.

Short amphiphilic peptides, in which a "tail" of apolar amino acids is flanked by a "head"

of charged residues can be thought as structurally akin to conventional surfactants and have been the object of systematic studies aimed at revealing structure-property relationships.[8,9] In water, the main driving force for self-assembly is the hydrophobic effect driving the non-polar amino acids to aggregate in order to minimize hydrophobic-water interaction. Like conventional surfactants, many amphiphilic peptides have displayed well-defined critical aggregation concentrations below which the monomeric solution state is favored. However, for some other experimental observations the picture of an equilibrium micellization is not appropriate. Instead, the self-assembly has been suggested to occur through crystallization with the processes of nucleation and growth of ordered aggregates.[10] Indeed, the most remarkable difference between the self-assembly of conventional surfactants and short amphiphilic peptides is the involvement of abundant hydrogen bonding interactions in the latter, in particular between the amide groups of peptide backbones. This typically leads to the formation of β-sheets extending along the direction of hydrogen bonding, that further order into one-dimensional nanostructures.[11]

The A_nK model peptides belong to this class of amphiphilic peptides, with a sequence of n hydrophobic alanine residues (A) and a single polar lysine residue (K) at the C terminus bearing a positively charged amino group, in addition to the unprotected N-terminus. Within the homologous series with n=6,8 and 10, the heptapeptide A_6K was shown to form hollow nanotubes above a critical aggregation concentration,[12] whereas the longer homologs A_8K and $A_{10}K$ self-assembled at progressively lower critical concentrations into twisted ribbons with a well-defined cross-section.[13] Despite the different overall morphology, the systems showed similar local packing of the peptides, which could be considered as laminated antiparallel β-sheets in a two-dimensional oblique crystal lattice.[14] In particular, the aggregation of A_8K and $A_{10}K$ into fibrils can be described as β-sheets extending in the direction of the fibril length axis, which laminate laterally by putting in contact their methyl group rich surfaces, due to the hydrophobic effect (Figure 1). The natural twisting of the chiral building blocks, which was appreciated experimentally in the ribbons, provides an explanation for the finite

cross section of the aggregates.[15,16] A simple model considering a free energy penalty due to stretching of hydrogen bonds within β-sheets arising from the twist of the ribbons, and an interfacial free energy gain of the hydrophobic β-sheets which would favor their lamination, was able to reasonably predict the optimal width of the twisted ribbons.[17]

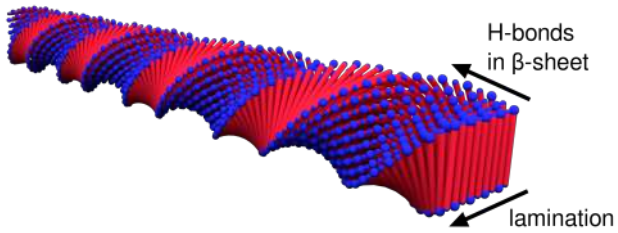

Figure 1 A schematic image showing the geometry of an A_nK peptide twisted ribbon consisting of 9 laminated β-sheets. The peptide molecule is represented as a red stick with two blue polar heads of different size. The directions in which the β-sheets extend in length and in which they laterally laminate are highlighted with arrows.

The characterization of the behavior of these peptides in a less polar solvent could be a way to probe the effect of the interfacial energy contribution of hydrophobic side chains exposed to the solvent considered in this model. Following an analogy between the amphiphilic peptides and the conventional surfactants one could hypothesize that the solvophobic effect in non-aqueous solvents should be weaker, resulting in an increase of the critical aggregation concentration[18–20] and a decrease of the equilibrium size of the aggregates.[21] In our investigation we considered the self-assembly of the peptides in two non-aqueous solvents: methanol (MeOH), which can be considered the first more hydrophobic analogue of water in which one hydrogen atom is replaced by a methyl group, and N,N-dimethylformamide (DMF), a solvent commonly used in peptide synthesis and considered to be "aprotic" since it is only a hydrogen bond acceptor.

Even if MeOH in some contexts can be considered a non-aggregating solvent,[22] this is not the case for peptide self-assembly. For a peptide containing a diphenylalanine moiety, a different molecular packing was observed, leading to a morphological transition from fibrils (water) to nanotubes (MeOH).[23,24] For "designer" peptides, which aggregate into β-sheet twisted fibrils, MeOH was observed to enhance β-sheet formation even at low concentrations,

at which the peptide was soluble in water as a random coil.[25] There is some interest in understanding peptide self-assembly also in organic solvents. This can tell us about the likely effect of a more hydrophobic environment on peptide self-assembly, with possible implications for the issue of lipid environments in amyloid fibrils formation.[26,27] Such knowledge can also expand the range of applications these peptidic building-blocks can be explored for.[28,29]

Methods

Sample preparation

The synthetic peptides A_nK (n=8, 10) were acquired from CPC Scientific Inc. as trifluoroacetate (TFA) stabilized salts with purities > 96 % and were used without further purification. Ultrapure water (MilliQ; Millipore), methanol (MeOH, purity 99.8 %, VWR chemicals) and N,N-dimethylformamide (DMF; purity 99.5 %, Fischer or RPE, ACS for analysis, Carlo Erba Reagents) were used as solvents. Weighted amounts of lyophilized peptides powders were solubilized with weighted amounts of solvents and the sample concentration was expressed in wt%, determined excluding the mass of the counterion. Unless otherwise specified, initial solutions were prepared at a concentration around 1 wt% and after 8 hours from the initial solubilization they were stepwise diluted to obtain the samples at lower concentration. For converting mass fractions to volume fractions (Table S1, Supporting Information), the value of the peptide densities in water previously reported[13] were assumed (1.50 $\mathrm{g\,cm^{-3}}$ for A_8K and 1.26 $\mathrm{g\,cm^{-3}}$ for $A_{10}K$) and the solvent densities at 25°C were used (d_{water}=0.997 $\mathrm{g\,cm^{-3}}$, d_{MeOH}=0.786 $\mathrm{g\,cm^{-3}}$ and d_{DMF} 0.948 $\mathrm{g\,cm^{-3}}$[30]).

SAXS experiments and data analysis

Small- and wide-angle X-ray scattering (SAXS/WAXS) measurements were performed on a Saxslab Ganesha pinhole instrument, JJ X-Ray System Aps, equipped with an X-ray microsource (Xenocs) and a two-dimensional 300k Pilatus detector (Dectris Ltd., Switzerland).

The X-ray wavelength was $\lambda = 1.54$ Å. Samples prepared at 1 wt% were measured in quartz capillary cells at room temperature in an evacuated chamber. Images were collected at three given sample-to-detector distances and the azimuthally averaged intensities as a function of the scattering vector $q = (4\pi/\lambda)sin(2\theta)$, where 2θ is the scattering angle, were subtracted for the contribution of the capillaries filled with solvent and put to absolute scale by calibration against water. Additional experiments on dilution series were performed at the SWING beamline of Synchrotron SOLEIL (Gif-sur-Yvette, France), with an X-ray wavelength $\lambda = 1.033$ Å. The sample-to-detector distance was 308 cm, allowing data collection in the scattering vector range $0.023 < q < 3.9$ nm^{-1}. The measurements were performed by loading the samples in disposable quartz capillaries with 2.0 mm diameter; scattering frames were collected with 10 exposures of 490 ms on an Eiger 4M detector (Dectris). The data collected on capillaries filled with solvent were used for subtraction. The SAXS data reduction (radial integration, absolute scaling, frames averaging, background subtraction) was performed using the FoxTrot software developed at the SOLEIL synchrotron. The subtracted scattering profiles on absolute scale were both analyzed by applying model-independent approaches (Guinier fit using Primus,[31] Indirect Fourier Transform using BayesApp[32]) and by fitting with the form factor of a long elliptical cylinder[33] with homogeneous electron density.[34]

CD measurements

Circular dichroism (CD) experiments were performed using a JASCO J-715 CD spectrometer. The spectra in the range $185 - 260$ nm were collected at room temperature with 1 nm band width, 2 s response time, and 20 nm min^{-1} scan rate. The average of three scans was used for each spectrum. Samples of A_8K and $A_{10}K$ at a concentration of 0.5 wt% in water and MeOH were placed in a 0.01 mm path length quartz cuvette (Hellma) for measurement. The solvent baseline was subtracted. Data in millidegrees were converted to units of mean residue ellipticity (deg dmol^{-1} cm^2) considering a peptide concentration of 0.005 gcm^{-3}, the

path length, the molecular weights (715 $\mathrm{g\,mol^{-1}}$ for A_8 and 857 $\mathrm{g\,mol^{-1}}$ for $A_{10}K$) and the number of residues (9 for A_8 and 11 for $A_{10}K$).

Cryo-EM experiments

Cryogenic electron microscopy imaging (Cryo-EM) was performed on a JEOL JEM-2200 instrument using a TVIPS F416 camera at the national Center for High Resolution Electron Microscopy within Lund University. An accelerator voltage of 200 kV was used. The samples were vitrified on lacey carbon film-covered copper grids using a Leica EM GP automatic plunge freezer. Grids used in all EM measurements were glow-discharged for increased wettability before sample preparation.

Light scattering measurements

Dynamic light scattering (DLS) experiments were performed with an ALV/DLS/SLS-5022F goniometer system with an ALV-7004 correlator at a scattering angle of 90°. The laser source was a 22 mW He–Ne laser with a wavelength of 632.8 nm. The samples were placed in 5 mm glass tubes, kept at 25°C and the intensity auto correlation functions were collected over runs of 300 s, using two Avalanche photodiode detectors operating in pseudo-cross correlation mode. Light scattering experiments were also performed using a modulated 3D light scattering instrument (LS instruments GmbH, Switzerland), implementing a laser with a wavelength of 660 nm and two Avalanche photodiodes. For the estimate of solubility, the mean count rate, at 90°, was obtained as the average of three subsequent runs of 100 s. The experimental intensity correlation functions $g^{(2)}(\tau)$ were converted to $C(\tau) = (g^{(2)}(\tau) - 1)/\beta = |g^{(1)}(\tau)|^2$,[35] where β is an instrumental constant, close to unity, and $g^{(1)}(\tau)$ is the correlation function of the electric field which was fitted using the cumulants expansion to obtain an average diffusion coefficient.[36] Fitting was performed with an in-house Matlab script.

Results and discussion

To study the self-assembly of A_8K and $A_{10}K$ in non-aqueous solvents and compare it to the behavior in water, an initial concentration of 1 wt% was chosen. Previous small-angle X-ray scattering experiments on the peptides in water[13,17] have shown that this concentration could be considered dilute enough not to show any effects of inter-aggregate interactions in the scattering profiles. The first observation made, was that the peptide samples in MeOH and DMF were more viscous than the corresponding samples in water prepared at similar concentrations and presented highly viscous (gel-like) states after $5 - 12$ hours from solubilization (Figure 2). Corresponding states have been observed for $A_{10}K$ samples in water only above a volume fraction of 0.02 (around 3 wt%).[37] Among the prepared samples, the 1 wt% $A_{10}K$ solution in MeOH also showed birefringence (Figure 2).

Figure 2 Arrested dynamics state of $A_{10}K$ (left) and A_8K (right) peptides in MeOH and DMF: photograph of 1 wt% peptide samples in vials after 1 week from direct preparation. In the inset, photograph of the $A_{10}K$ 1 wt% sample in MeOH between cross-polarizers.

SAXS experiments (Figure 3) showed very similar scattering profiles in the three solvents, indicating that aggregates formed in MeOH and DMF essentially have the same ribbon morphology as in water.[13,17] A correlation peak in the lower q range was observed for the samples in MeOH and DMF, whereas this feature was absent in the water samples (Figure 3A and C). This observation testifies the presence of characteristic distances in the fibrils suspension arising from inter-aggregates interactions, suggesting that the samples in MeOH and DMF, at these concentrations (volume fraction around 0.006), are not in the dilute regime, but rather in the semi-dilute, borrowing terminology from the theoretical framework for polyelectrolytes.[38,39] Synchrotron SAXS experiments on dilution series for A_8K and $A_{10}K$ in

MeOH confirmed that the correlation peak disappears at low enough concentration (insets in Figure 3A,C and Figure S1, Supplementary information). Therefore, the SAXS data collected for samples in MeOH and DMF at concentration below 0.25 wt%, in the low q regime, clearly present the q^{-1} slope characteristic of rigid rod-like objects and could be interpreted in terms of a particle form factor similarly to what has been suggested[17] for 1 wt% samples of A_8K and $A_{10}K$ in water (Figure 3B,D and Table S2, Supporting Information).

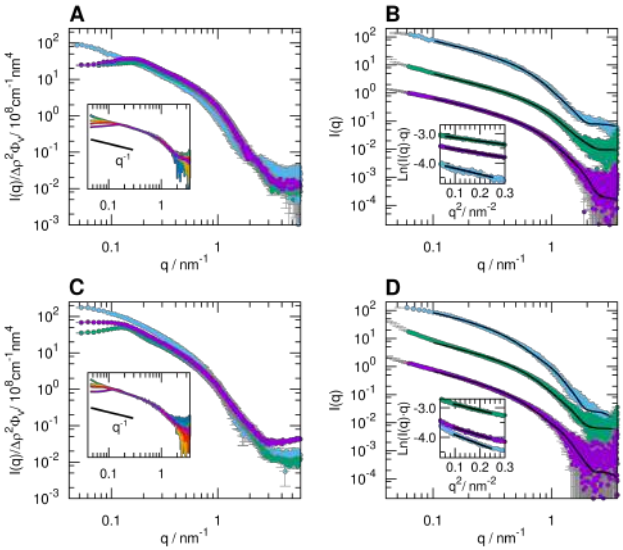

Figure 3 SAXS profiles of A_8K (A), and of $A_{10}K$ (C) in water (blue), MeOH (green) and DMF (purple). The peptide concentration is around 1 wt% and the scattered intensity in cm^{-1} is divided by the estimated peptide volume fraction and by the squared scattering length density difference $\Delta\rho^2$, in nm^{-4}. In the insets, SAXS profiles of A_8K and $A_{10}K$ solutions in MeOH at concentrations of 1 wt% (purple), 0.5 wt% (red), 0.25 wt% (orange), 0.125 wt% (green), and 0.0625 wt% (blue) are reported. The data were multiplied by a scaling constant chosen to ensure superimposition in the q range $0.635 - 1.227$ nm^{-1} (listed in Table S1, Supporting Information, together with concentration values). SAXS experimental data at peptide concentration of 1 wt% in water (blue) and 0.125 wt% in MeOH (green) and DMF (purple) are reported for A_8K and $A_{10}K$ in panels B and D, respectively, along with the calculated curve based on the form factor of a cylinder with elliptical cross section (black lines) and the Guinier fits for rod-like objects in the insets. The curves are shifted by a convenient factor to avoid overlapping. The optimized parameters of the calculated curves are shown in Table S2, Supporting Information.

The SAXS data could therefore be described by means of the form factor of an elliptical cylinder[33] whose length was set to a value beyond the maximum distance accessible with the available minimum q, except for the $A_{10}K$ fibrils in water which had already shown to have a shorter length, around 60 nm, when prepared at this concentration (Table S2, Supporting Information).[13,17] The optimized values for the cross-section semi-axes agree

with an approximate diameter of 6 nm, as previously reported.[13,17,37]

However, when inspecting the parameters obtained by fitting several experimental data, we consistently detected slightly smaller cross-section sizes for the aggregates of the same peptide in the non-aqueous solvents compared to water. This observation of a smaller average cross-section was confirmed by estimating the radius of gyration of the cross-section, R_{CS}, by applying a Guinier fit for rod-like objects (insets in Figure 3B,D and Table S3, Supporting Information). A second estimate of the same parameter could be derived from the pair distance distribution function of the cross-section (Figure S2, Supporting Information) obtained by indirect Fourier transform of the $I(q)q$ vs. q curve, at $q > 0.3$ nm^{-1}.

Some geometrical considerations can be made based on the assumption that the fibril cross section is given by the lamination of a constant number of extended peptide molecules. In the model used for fitting the SAXS data the cross-section of the aggregates is approximated as a homogeneous ellipse of semi-axes a and b. The smaller axis, $2a$, would represent the cross-section thickness and considered equal to the length of the fully extended peptide, estimated as 3.2 nm for A_8K and 3.9 nm for $A_{10}K$. The cross-section width, $2b$, should be given by the number of laminated β-sheets times the separation between them, estimated to be 0.54 nm.[14] Considering how the radius of gyration depends on the semi axes a and b of a homogenous elliptical cross section $R_{CS} = (a^2 + b^2)^{(1/2)}/2$,[40] we tried to estimate the fibril width (Table S3, Supporting Information). These estimates would suggest that the number of laminated β-sheets in the fibrils decreases to approximately 80% and 90% of the value in water in MeOH and DMF, respectively. The difference between the average fibril cross-section radius of gyration in water and MeOH, although small, can be considered statistically relevant; a different slope of the scattering profile in the q region $0.3 - 0.5$ nm^{-1} is clearly observable (Figure 3B,D insets).

The simplified model invoked to explain the finite and monodisperse cross section of the A_8K and $A_{10}K$ ribbons[17] was based on a trade-off between the surface energy gain with lamination of the apolar alanine-rich sheets and the energy penalty given by increased

distortion of the hydrogen bonds within the β-sheets. A smaller optimal number of laminated β-sheets in a solvent with lower interfacial tension than water towards a hydrophobic surface (Table 1) would qualitatively agree with this interpretation.

However, the approximation of the peptide ribbons as a homogeneous cylinder with elliptical cross-section neglects both possible electron density variations at the surface of the ribbons and their twisted nature. In particular, the first approximation can be problematic in the comparison between peptide fibrils in water and other solvents due to the complex description of an interface towards the bulk solvent which includes solvation layers and counterions. It is known that proteins in water have a first hydration shell with electron density $\approx 10\%$ higher than the bulk solvent.[41] A similar interfacial effect could occur on the surface of the peptide ribbons in water determining a slight overestimation of the cross-section assuming the simple homogeneous electron density model, compared to the true geometrical size of the assembled peptide aggregates. On the other hand, it could be estimated that undissociated counterions should be present to a larger extent at the surface of the peptide ribbons in the solvents with a lower dielectric constant than water, due to stronger coulombic attraction (Table 1). One can predict that the presence of undissociated counterions should also increase the cross-section deduced from the SAXS data compared to the geometrical size of the bare peptide fibrils, whereas the observed values are smaller than those in water. Overall, due to the approximations in the model adopted to describe the SAXS data, we can conclude that the ribbons formed by the self-assembly of A_8K and $A_{10}K$ in MeOH and DMF have a very similar or only slighter smaller cross-section compared to the aggregates formed in water.

Concerning the local packing of the peptides within the ribbons, previously reported x-ray scattering data in the wide-angle range for A_8K and $A_{10}K$ in water, at concentrations 2-3 wt%, showed three distinguishable peaks at q values 11.8, 14.3 and 16.1 nm^{-1}.[13] These three Bragg reflections have been indexed to an oblique 2D lattice[14] resembling the molecular packing within polyalanine crystals.[42] The WAXS data collected on $A_{10}K$ in MeOH, at

1 wt%, clearly showed three Bragg peaks at the same position as in water, suggesting the same molecular packing within the fibrils formed in the non-aqueous solvent (Figure 4D) and confirming its crystalline nature. The lower peptide concentration compared to previously published data and the presence of the broad solvent scattering peak having its maximum in the same q region where the reflections occur (centered around 13 nm^{-1} for DMF and 16 nm^{-1} for MeOH, whereas it is found around 20 nm^{-1} for water), made the WAXS peaks of the aggregates in the non-aqueous solvents experimentally more difficult to resolve, particularly for the samples in DMF. Some excess signal compared to the solvent in the q region 10-18 nm^{-1} could be evidenced for these samples, with the most intense maximum around 14 nm^{-1} (Figure S3, Supporting Information).

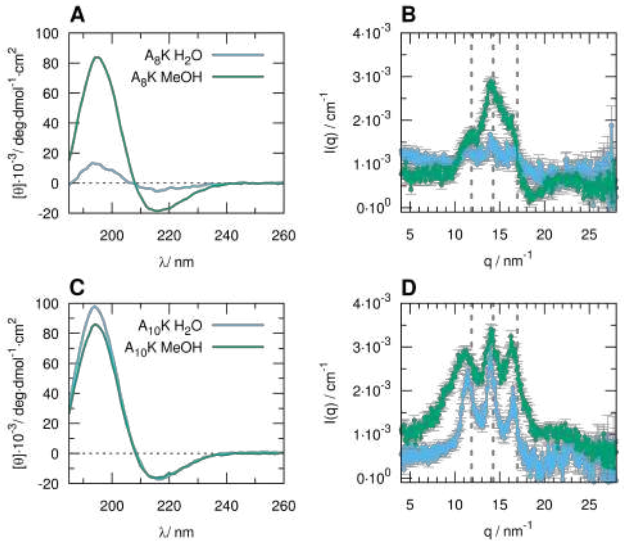

Figure 4 Circular dichroism spectra of 0.5 wt% A_8K (A) and $A_{10}K$ (C) solutions in water (blue line) and in MeOH (green line). WAXS data of 1 wt% A_8K (B) and $A_{10}K$ (D) solutions in water (blue) and MeOH (green). The positions of reference Bragg peaks reported in the literature[13,14] are marked with vertical dashed lines in panels B and D.

For the A_8K and $A_{10}K$ fibrils formed in MeOH it was also possible to obtain reliable CD data, whereas for the samples in DMF the solvent absorption in the far UV hampered the use of this spectroscopic technique. The CD spectra (Figure 4A,C) showed the characteristic positive band at $\lambda = 195$ nm and a negative band at $\lambda = 215$ nm, already observed for the peptide aggregates in water and consistent with a β-sheet peptide arrangement.[43] It

could be noticed that at 0.5 wt% peptide concentration the CD signal arising from the A_8K aggregates in water is much weaker than in MeOH. This already suggests a lower solubility of this peptide as monomer in MeOH compared to water, resulting in a higher aggregate concentration. This is further investigated below.

Length of peptide fibrils

From the data presented in the previous section we could appreciate that A_8K and $A_{10}K$ form in MeOH fibrillar aggregates with the same local packing as in water, possibly with a slightly smaller cross-section. Cryo-TEM experiments confirmed that similar kind of fibrils form in water and MeOH for both A_8K (Figure 5A,B) and $A_{10}K$ (Figure 5C,D). The aggregates have an estimated cross section of approximately 4 nm (Figure S4, Supporting Information), consistent with the SAXS experiments. The images overall suggest that the fibrils of both peptides grow longer in MeOH compared to those in water. This is consistent with the observation that at the same peptide mass concentration, solutions are more viscous in MeOH than in water (Figure 2).

DLS was used to compare the length of the aggregates in the different solvents and to detect the slowing down of the dynamics above the overlap concentration of aggregates. The normalized intensity autocorrelation functions, $C(t)$, are shown in Figure 6. At low concentrations the correlation function is approximately unimodal, and an average diffusion coefficient, $\overline{D}$, can be obtained using the method of cumulants.[36] The relaxation is assumed to be purely diffusive and can be interpreted as a weighted average of the parallel and perpendicular translational modes, giving rise to an average diffusion coefficient $D_t = 1/3D_{\|} + 2/3D_{\perp}$.[44] From the obtained values of the diffusion coefficient an average length can be estimated from the equations proposed by Broersma.[45,46] By assuming viscosity values of $\eta_{\text{water}} = 0.891$ cP, $\eta_{\text{MeOH}} = 0.485$ cP and $\eta_{\text{DMF}} = 0.802$ cP, and the diameter of the cross-section obtained by SAXS data fits, we obtained a Z-averaged length of about 200 nm in water, 800 nm in MeOH

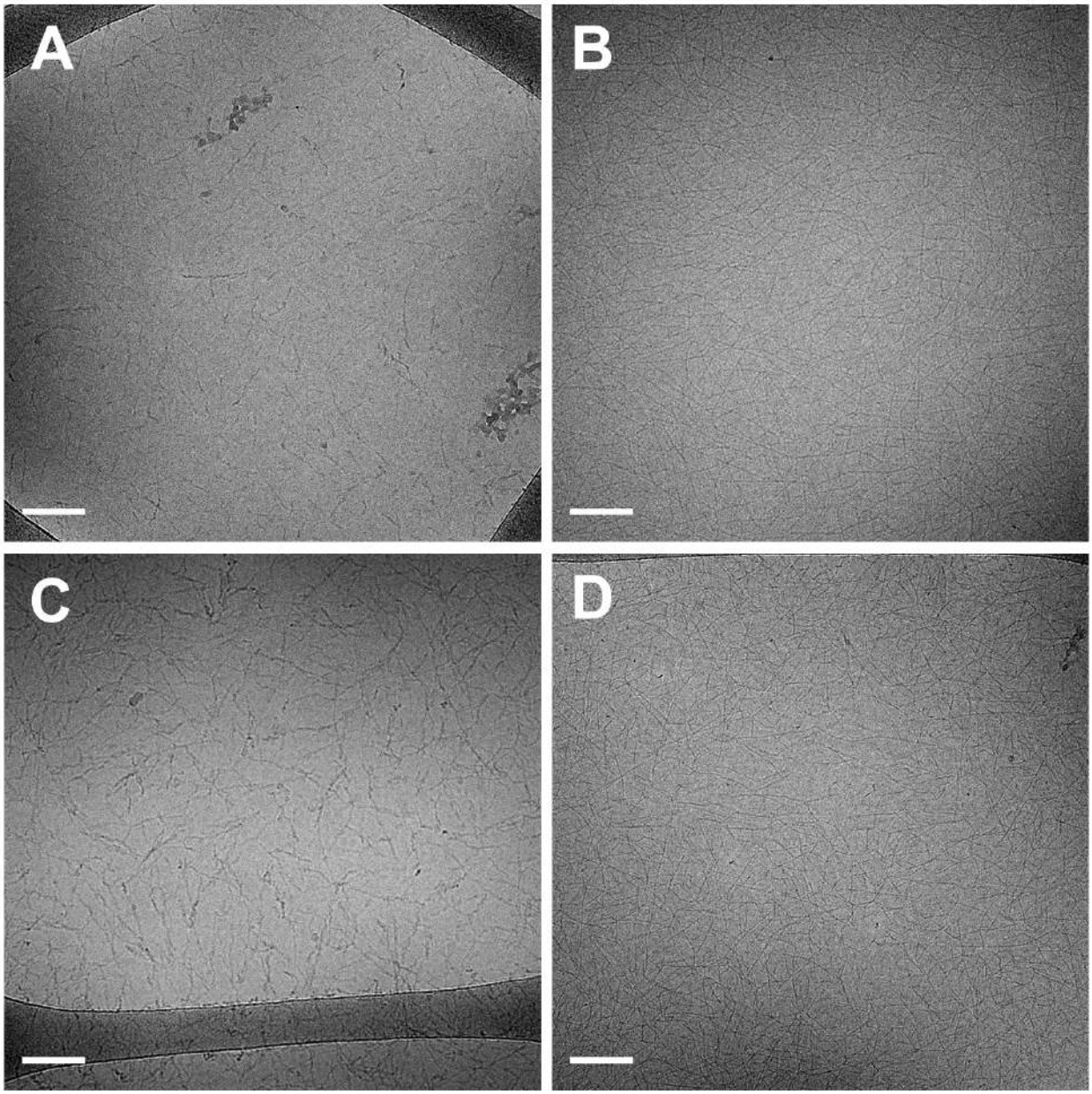

Figure 5 Cryo-TEM images for A_8K 0.05 wt% in water (A), A_8K 0.01 wt% in MeOH (B), $A_{10}K$ 0.02 wt% in water (C) and $A_{10}K$ 0.01 wt% in MeOH (D). All scale bars are 100 nm.

and 1000 nm in DMF. At the highest concentration, 0.50 wt%, in MeOH and DMF, a slow mode is observed in the correlation function. This signals the onset of dynamic arrest and that the system is trapped in a non-ergodic glassy state. The same effect is also observed in water, but at concentration ≥ 1 wt%.[13,37] Reasonably, this transition occurs at a lower concentration in MeOH and DMF due to the longer aggregates formed in these solvents.

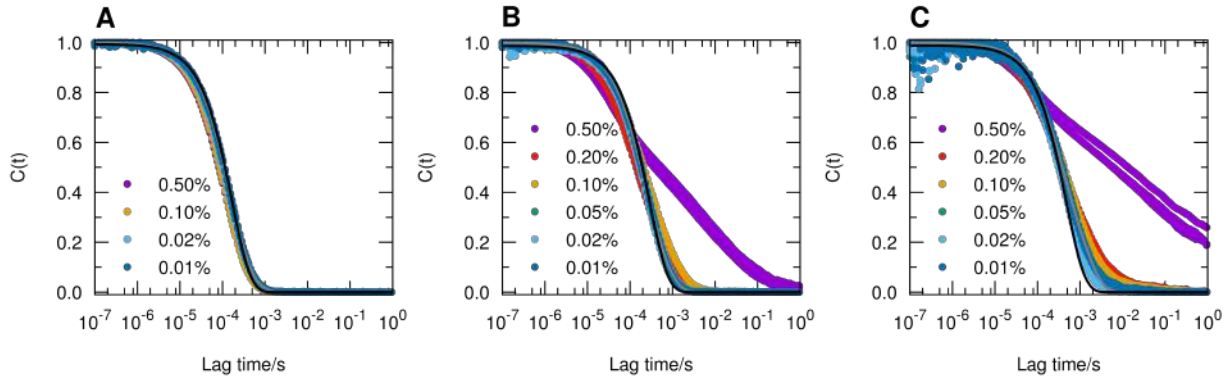

Figure 6 Normalized intensity auto-correlation functions of $A_{10}K$ peptide aggregates in water (A), MeOH (B) and DMF (C) as a function of concentration. For the most dilute samples, the data could be described as a double exponential decay (grey line) or using the method of cumulants with an average diffusion coefficient of 8.6, 5.0 and 2.7×10^{-12} m^2s^{-1} in water, in MeOH and in DMF, respectively (black lines).

Monomer solubility and driving force for self-assembly

Aggregates begin to form above a particular concentration, that can be interpreted as the monomer solubility, c_s. This concentration can be measured *e.g.* by following the scattered light intensity as a function of dilution of a sample with an initial concentration $c > c_s$.[13] For this purpose solutions of the peptides at 1 wt% were gradually diluted in order to determine at which concentration the light scattering signal reached the solvent level, which is a good indication of the monomer solubility. Whith this method, monomer solubilities in water of 2 mM and 7 μM were determined for A_8K and $A_{10}K$, respectively.[13] Scattered intensity data for MeOH and DMF are presented in Figure 7. For A_8K, monomer solubilities of about 10 μM were obtained, meaning approximately two orders of magnitude smaller compared to that in water. Interestingly, approximately the same solubilities were obtained for $A_{10}K$ in

these solvents. Hence, for this peptide we found approximately the same c_s in water, MeOH and DMF.

In water, c_s of $A_{10}K$ is almost two orders of magnitude smaller than the c_s of A_8K. This can be attributed to the hydrophobic effect.[13] In MeOH and DMF, the hydrophobic interaction is significantly reduced. Here, instead we need to consider the capability to solvate ions, *i.e.* the charges of the monomers and the TFA counterions, and the possibility of the solvents to hydrogen bond to the peptide amide groups.

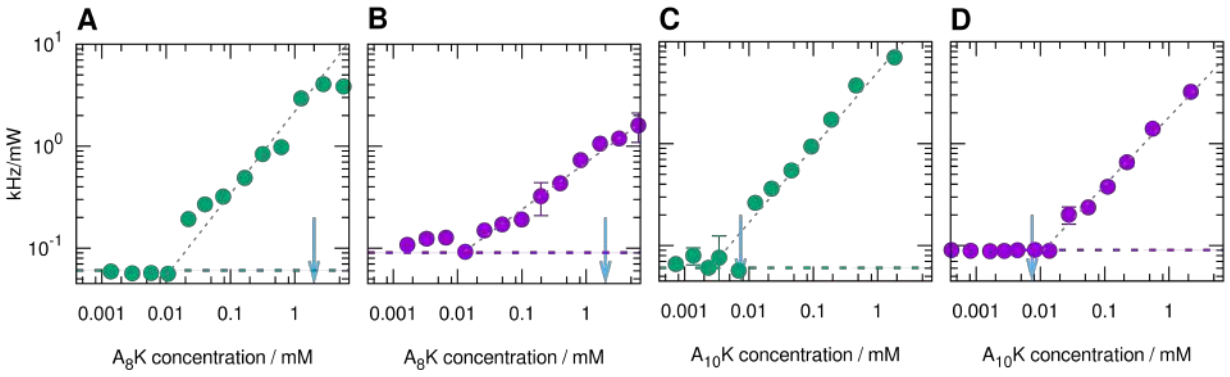

Figure 7 Variation of the scattered light intensity with peptide concentration for A_8K in MeOH (A) and DMF (B), and for $A_{10}K$ in MeOH (C) and DMF (D). The values of the solubility in water estimated with the same approach (from Ref.[13]) are indicated for comparison with blue arrows. The signal measured for the pure solvent is shown as a horizontal dashed line. The grey dashed lines represent a guide for the eye.

The structural similarity among the A_8K and $A_{10}K$ aggregates formed in water, MeOH and DMF would suggest a similar energetic state of the peptide molecules within the fibrils, almost independent on the surrounding solvent. Therefore, the increased relative stability of the aggregates in the non-aqueous solvents suggested by the lower solubility of A_8K and enhanced fibril growth should be due to a destabilization of the monomer state in solution when changing solvent from water to MeOH or DMF.

The driving force for the formation of the fibrillar aggregates of these amphiphilic peptides could be thought in terms of three different energetic contributions: hydrophobic interactions, electrostatic interactions and ion solvation, and hydrogen bonds.[7,47] In water the aggregation of A_8K and $A_{10}K$ is mainly driven by hydrophobic interaction between the alanine amino acids, as reflected in the significant lower solubility of $A_{10}K$, which has two hydrophobic

alanine residues more than A_8K. In MeOH and DMF, on the other hand, solubilities are similar. This indicates that it is rather the hydrogen bonding capacity and electrostatics that determines the monomer solubility, properties that are similar for the two peptides.

Table 1 Some physico-chemical properties of the three solvents in which the self-assembly of the peptides was investigated.

Property	**H_2O**	**MeOH**	**DMF**
Solubility of NaCl at 25°C (g/l)[48]	359	14.9	4
Solubility of hexane at 25°C (g/l)[49,50]	0.0124	604	–
Dielectric constant at 25°C[51]	78.3	32.6	36.7
Dipole moment (Debye)[51]	1.85	1.70	3.82
CMC of SDS at 25°C (nM)[52,53]	7.8	6.9	14.62
Surface tension at 25°C (dynes/cm)[54]	72.70	22.10	34.40
Hansen solubility parameter (H-bond) δ_H (J/cm^3)[55]	42.3	22.3	11.3

We can schematically consider how the change of solvent properties, presented in Table 1, when moving from water to slightly less polar MeOH and DMF, can affect the different energetic contributions to fibril formation.

Electrostatic interaction between ions is expected to increase in magnitude when changing solvent from water to MeOH and DMF, due to a lowering of the dielectric constant. This effect should increase the repulsion between the charged peptide molecules and thereby hinder the aggregation. This is not observed in our case where aggregates form and grow even longer in MeOH than in water. It is reasonable that a lower solvating ability of MeOH and DMF towards the charged groups of the peptides and the TFA counterions can lower the ionization degree of the peptides in these solvents, thereby decreasing the peptide-peptide repulsion and favoring the aggregation.

Less polar solvents are expected to decrease the surface energy of the apolar alanine side chains reducing the solvophobic contribution to the self-assembly, which mainly affects the lateral lamination. This phenomenon could explain the slightly smaller optimum number of laminated β-sheets deduced from the fibrils cross-section in the less polar solvents MeOH and DMF.

Solvents like MeOH or DMF are less prone than water to hydrogen bonding with the

peptide monomer. In these non-aqueous solvents, the inter-peptide hydrogen bond formation within the fibril provides a notable energy gain and becomes a key driving force to the peptide assembly into ribbons, especially in the longitudinal direction.

The less favorable hydrogen bonding between peptide and solvent molecules in MeOH and DMF compared to water could also have an impact on the kinetics of fibril growth. The slow kinetics observed for reaching a steady-state for the aggregation of $A_{10}K$ fibrils in water would be in agreement with their crystalline nature, which implies a formation mechanism with nucleation and growth. These are both activated processes, for which the energy barrier also involves the replacement of hydrogen bonds for a successful docking of the peptide within the β-sheets.[56] In this view, the growth of peptide fibrils in length, with elongation of the β-sheets, should also proceed faster in MeOH and DMF. The observation of "enhanced growth" of the peptide fibrils in these solvents probably includes both thermodynamics and kinetics aspects.

Fibril-fibril interactions

The peak observed in the low q range in the SAXS profiles for the peptides in MeOH and DMF at the higher concentrations, together with the slow relaxation in DLS experiments suggested that inter-particle interactions are not negligible in this concentration regime. This is in contrast to aqueous samples, where similar peptide mass concentrations could still be considered dilute in the SAXS data interpretation.[13,17,57] Inter-particle interactions can be quantified in terms of an effective structure factor, $S_{eff}(q)$, that can be obtained from scattering data, by dividing the experimental scattering curve with the experimental form factor measured at high dilution, where $S_{eff}(q) \approx 1$.[58] In particular, for a binary system, $S_{eff}(0)$ reports on the osmotic compressibility, $S_{eff}(0) = k_{\mathrm{B}}T/V_{\mathrm{p}}(\partial\Pi/\partial\phi)^{-1}$, where Π is the osmotic pressure and V_{p} is the particle volume. In Figure 8 we have plotted $S_{eff}(q)$, for A_8K and $A_{10}K$ in MeOH for three concentrations, 0.25, 0.5 and 1.0 wt%. As can

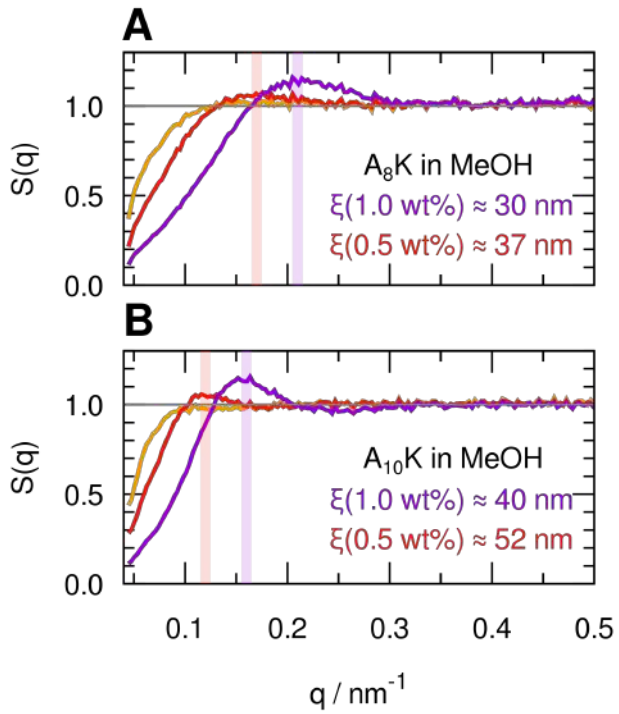

Figure 8 Experimental structure factors of the A_8K (A) and $A_{10}K$ (B) samples in MeOH at concentrations 1 wt% (purple), 0.5 wt% (red) and 0.25 wt% (orange), estimated as the ratio between the SAXS profiles of the samples at higher concentration and that of the sample at 0.12 wt%, which could be identified with the form factor of the aggregates. Correlation lengths estimated from the q_{peak} positions as $\xi = 2\pi/q_{\mathrm{peak}}$ are reported.

be seen, $S_{eff}(0)$ decreases with increasing concentration demonstrating that interaggregate interactions are predominantly repulsive. Interestingly, $S_{eff}(0)$ is indeed significantly lower in MeOH compared to in water (see Figure 3A,C). The reason for this is not fully clear.

We expect a stronger counterion condensation in MeOH due to the lower dielectric constant, and hence a weaker electrostatic repulsion. However, changes of the potential at the surface of the charged fibrils, involving the protonation state of the ionizable groups, counterions and solvation effects, are difficult to predict. For A_8K in water, a pH decrease as a function of the increasing concentration has been observed, compatible with a partial deprotonation of the peptides being involved in the formation of the aggregates.[59] This aspect might change when the petides self-assemble in a non-aqueous solvent. In any case, a stronger steric excluded volume repulsion in MeOH is expected due to the longer aggregates and their increased overlap.[37]

The peak in $S_{eff}(q)$ reports essentially on the mesh size of the network, $\xi \approx D/\phi^{(1/2)}$, where D is the effective aggregate diameter (≈ 5 nm) and ϕ is the volume fraction. Experimental estimates of ξ can be obtained from $\xi = 2\pi/q_{\max}$, where $q_{\max}$ is the position of the structure factor peak. The stimated values (Figure 8) agree reasonably well with the simple formula for ξ, and as expected, ξ decreases with increasing concentration.

Conclusion

We have shown that the model peptides A_8K and $A_{10}K$ self-assemble into similar ribbon-like aggregates in both MeOH and DMF, as in water. However, in the case of A_8K self-assembly begins at roughly 100 times lower concentrations in MeOH and DMF, compared to water. We attribute this decrease to a lower degree of hydrogen bonding in the non-aqueous solvents, so that the formation of inter-peptide hydrogen bonds in fibril formation becomes a relevant driving force to aggregation.

As in water, dynamic light scattering experiments indicate a dramatic slowing down of

dynamics in MeOH and DMF as the ribbon-like aggregates overlap and form a glassy state. This also occurs at lower mass concentration, compatibly with the idea that fibrils formed in the non-aqueous solvents grow longer. Finally, repulsive inter-particle interactions are stronger in the non-aqueous solvents compared to in water. The reason for this is not yet fully understood.

Acknowledgement

This research is funded by the *Knut and Alice Wallenberg Foundation*, grant number KAW 2014.0052. Parts of this research were carried out at the SWING beamline at SOLEIL. We would like to thank J. Perez for assistance during the experiment. This work benefited from the use of the SasView application, originally developed under NSF award DMR-0520547. SasView contains code developed with funding from the European Union's Horizon 2020 research and innovation programme under the SINE2020 project, grant agreement No 654000.

References

(1) Chiti, F.; Dobson, C. M. Protein Misfolding, Amyloid Formation, and Human Disease: A Summary of Progress Over the Last Decade. *Annual Review of Biochemistry* **2017**, *86*, 27–68.

(2) Otzen, D.; Riek, R. Functional Amyloids. *Cold Spring Harbor Perspectives in Biology* **2019**, a033860.

(3) Hartgerink, J. D.; Beniash, E.; Stupp, S. I. Self-assembly and mineralization of peptide-amphiphile nanofibers. *Science* **2001**, *294*, 1684–1688.

(4) Zhao, X.; Pan, F.; Xu, H.; Yaseen, M.; Shan, H.; Hauser, C. A.; Zhang, S.; Lu, J. R. Molecular self-assembly and applications of designer peptide amphiphiles. *Chemical Society Reviews* **2010**, *39*, 3480–3498.

(5) Schneider, J. P.; Pochan, D. J.; Ozbas, B.; Rajagopal, K.; Pakstis, L.; Kretsinger, J. Responsive hydrogels from the intramolecular folding and self-assembly of a designed peptide. *Journal of the American Chemical Society* **2002**, *124*, 15030–15037.

(6) Zapadka, K. L.; Becher, F. J.; Gomes dos Santos, A. L.; Jackson, S. E. Factors affecting the physical stability (aggregation) of peptide therapeutics. *Interface Focus* **2017**, *7*.

(7) Dill, K. A. Dominant Forces in Protein Folding. *Biochemistry* **1990**, *29*, 7133–7155.

(8) Hamley, I. W. Self-assembly of amphiphilic peptides. *Soft Matter* **2011**, *7*, 4122–4138.

(9) Zhao, Y.; Yang, W.; Chen, C.; Wang, J.; Zhang, L.; Xu, H. Rational design and self-assembly of short amphiphilic peptides and applications. *Current Opinion in Colloid and Interface Science* **2018**, *35*, 112–123.

(10) Cenker, Ç. Ç.; Bomans, P. H.; Friedrich, H.; Dedeoğlu, B.; Aviyente, V.; Olsson, U.; Sommerdijk, N. A.; Bucak, S. Peptide nanotube formation: A crystal growth process. *Soft Matter* **2012**, *8*, 7463–7470.

(11) Aggeli, A.; Bell, M.; Boden, N.; Keen, J. N.; Knowles, P. F.; McLeish, T. C.; Pitkeathly, M.; Radford, S. E. Responsive gels formed by the spontaneous self-assembly of peptides into polymeric β-sheet tapes. *Nature* **1997**, *386*, 259–262.

(12) Bucak, S.; Cenker, C.; Nasir, I.; Olsson, U.; Zackrisson, M. Peptide nanotube nematic phase. *Langmuir* **2009**, *25*, 4262–4265.

(13) Cenker, C. C.; Bucak, S.; Olsson, U. Aqueous self-assembly within the homologous peptide series AnK. *Langmuir* **2014**, *30*, 10072–10079.

(14) Kuczera, S.; Rüter, A.; Roger, K.; Olsson, U. Two dimensional oblique molecular packing within a model peptide ribbon aggregate. *ChemPhysChem* **2020**,

(15) Nyrkova, I. A.; Semenov, A. N.; Aggeli, A.; Boden, N. Fibril stability in solutions of twisted β-sheet peptides: A new kind of micellization in chiral systems. *European Physical Journal B* **2000**, *17*, 481–497.

(16) Aggeli, A.; Nyrkova, I. A.; Bell, M.; Harding, R.; Carrick, L.; McLeish, T. C. B.; Semenov, A. N.; Boden, N. Hierarchical self-assembly of chiral rod-like molecules as a model for peptide -sheet tapes, ribbons, fibrils, and fibers. *Proceedings of the National Academy of Sciences* **2001**, *98*, 11857–11862.

(17) Rüter, A.; Kuczera, S.; Pochan, D. J.; Olsson, U. Twisted Ribbon Aggregates in a Model Peptide System. *Langmuir* **2019**, *35*, 5802–5808.

(18) Ceglie, A.; Colafemmina, G.; Della Monica, M.; Olsson, U.; Jönsson, B. Shape and Size of Micelles in the Sodium Dodecyl Sulfate-Formamide System. *Langmuir* **1993**, *9*, 1449–1455.

(19) Wärnheim, T. Aggregation of surfactants in nonaqueous, polar solvents. *Current Opinion in Colloid and Interface Science* **1997**, *2*, 472–477.

(20) Wijaya, E. C.; Separovic, F.; Drummond, C. J.; Greaves, T. L. Micelle formation of a non-ionic surfactant in non-aqueous molecular solvents and protic ionic liquids (PILs). *Physical Chemistry Chemical Physics* **2016**, *18*, 24377–24386.

(21) Lonetti, B.; Tsigkri, A.; Lang, P. R.; Stellbrink, J.; Willner, L.; Kohlbrecher, J.; Lettinga, M. P. Full characterization of PB-PEO wormlike micelles at varying solvent selectivity. *Macromolecules* **2011**, *44*, 3583–3593.

(22) Di Gregorio, M. C.; Severoni, E.; Travaglini, L.; Gubitosi, M.; Sennato, S.; Mura, F.; Redondo-Gómez, C.; Jover, A.; Pavel, N. V.; Galantini, L. Bile acid derivative-based catanionic mixtures: Versatile tools for superficial charge modulation of supramolecular lamellae and nanotubes. *Physical Chemistry Chemical Physics* **2018**, *20*, 18957–18968.

(23) Castelletto, V.; Hamley, I. W.; Harris, P. J.; Olsson, U.; Spencer, N. Influence of the solvent on the self-assembly of a modified amyloid beta peptide fragment. I. Morphological investigation. *Journal of Physical Chemistry B* **2009**, *113*, 9978–9987.

(24) Krysmann, M. J.; Castelletto, V.; McKendrick, J. E.; Clifton, L. A.; Harris, P. J. F.; King, S. M.; King, S. M. Self-Assembly of Peptide Nanotubes in an Organic Solvent. *Langmuir* **2008**, *24*, 8158–8162.

(25) Davies, R. P. W.; Aggeli, A. Self-assembly of amphiphilic β-sheet peptide tapes based on aliphatic side chains. *Journal of Peptide Science* **2011**, *17*, 107–114.

(26) Gaspar, R.; Pallbo, J.; Weininger, U.; Linse, S.; Sparr, E. Ganglioside lipids accelerate α-synuclein amyloid formation. *Biochimica et Biophysica Acta - Proteins and Proteomics* **2018**, *1866*, 1062–1072.

(27) Galvagnion, C.; Topgaard, D.; Makasewicz, K.; Buell, A. K.; Linse, S.; Sparr, E.; Dobson, C. M. Lipid Dynamics and Phase Transition within α-Synuclein Amyloid Fibrils. *Journal of Physical Chemistry Letters* **2019**, *10*, 7872–7877.

(28) Mason, T. O.; Chirgadze, D. Y.; Levin, A.; Adler-Abramovich, L.; Gazit, E.; Knowles, T. P.; Buell, A. K. Expanding the solvent chemical space for self-assembly of dipeptide nanostructures. *ACS Nano* **2014**, *8*, 1243–1253.

(29) Zhao, Y.; Deng, L.; Wang, J.; Xu, H.; Lu, J. R. Solvent Controlled Structural Transition of KI4K Self-Assemblies: From Nanotubes to Nanofibrils. *Langmuir* **2015**, *31*, 12975–12983.

(30) Lemmon, E.; McLinden, M.; Friend, D. In *NIST Chemistry WebBook, NIST Standard Reference Database NUmber 69*; Linstrom, P. J., Mallard, W., Eds.; National Institute of Standards and Technology: Gaithersburg MD, 2020.

(31) Konarev, P. V.; Volkov, V. V.; Sokolova, A. V.; Koch, M. H. J.; Svergun, D. I. PRIMUS : a Windows PC-based system for small-angle scattering data analysis. *Journal of Applied Crystallography* **2003**, *36*, 1277–1282.

(32) Hansen, S. BayesApp : a web site for indirect transformation of small-angle scattering data. *Journal of Applied Crystallography* **2012**, *45*, 566–567.

(33) Pedersen, J. S. Analysis of small-angle scattering data from colloids and polymer solutions: Modeling and least-squares fitting. *Advances in Colloid and Interface Science* **1997**, *70*, 171–210.

(34) http://www.sasview.org/.

(35) Schätzel, K. Correlation techniques in dynamic light scattering. *Applied Physics B Photophysics and Laser Chemistry* **1987**, *42*, 193–213.

(36) Koppel, D. E. Analysis of macromolecular polydispersity in intensity correlation spectroscopy: The method of cumulants. *The Journal of Chemical Physics* **1972**, *57*, 4814–4820.

(37) Rüter, A.; Kuczera, S.; Gentile, L.; Olsson, U. Arrested dynamics in a model peptide hydrogel system. *Soft Matter* **2020**, *16*, 2642–2651.

(38) De Gennes, P.; Pincus, P.; Velasco, R.; Brochard, F. Remarks on polyelectrolyte conformation. *Journal de Physique* **1976**, *37*, 1461–1473.

(39) Salamon, K.; Aumiler, D.; Pabst, G.; Vuletić, T. Probing the mesh formed by the semirigid polyelectrolytes. *Macromolecules* **2013**, *46*, 1107–1118.

(40) Glatter, O.; Kratky, O. *Small angle X-ray scattering*; Academic Press: London, 1982.

(41) Svergun, D. I.; Richard, S.; Koch, M. H.; Sayers, Z.; Kuprin, S.; Zaccai, G. Protein hydration in solution: experimental observation by x-ray and neutron scattering. *Proceedings of the National Academy of Sciences of the United States of America* **1998**, *95*, 2267–2272.

(42) Asakura, T.; Okonogi, M.; Horiguchi, K.; Aoki, A.; Saitô, H.; Knight, D. P.; Williamson, M. P. Two different packing arrangements of antiparallel polyalanine. *Angewandte Chemie - International Edition* **2012**, *51*, 1212–1215.

(43) Kelly, S. M.; Jess, T. J.; Price, N. C. How to study proteins by circular dichroism. *Biochimica et Biophysica Acta - Proteins and Proteomics* **2005**, *1751*, 119–139.

(44) Berne, B.; Pecora, R. *Dynamic Light Scattering: With Applications to Chemistry, Biology, and Physics*; John Wiley & Sons: New York, NY (USA), 1976; p 376.

(45) Broersma, S. Viscous Force Constant for a Closed Cylinder. *The Journal of Chemical Physics* **1960**, *32*, 1632–1635.

(46) Broersma, S. Viscous force and torque constants for a cylinder. *The Journal of Chemical Physics* **1981**, *74*, 6989–6990.

(47) Klotz, I. M.; Franzen, J. S. Hydrogen Bonds between Model Peptide Groups in Solution. *Journal of the American Chemical Society* **1962**, *84*, 3461–3466.

(48) Burgess, J. *Metal Ions in Solution*; Ellis Horwood: New York, 1978.

(49) Polak, J.; Lu, B. C.-Y. Mutual Solubilities of Hydrocarbons and Water at 0 and 25 °C. *Canadian Journal of Chemistry* **1973**, *51*, 4018–4023.

(50) Kiser, R. W.; Johnson, G. D.; Shetlar, M. D. Solubilities of Various Hydrocarbons in Methanol. *Journal of Chemical and Engineering Data* **1961**, *6*, 338–341.

(51) Lide, D. R., Ed. *CRC Handbook of Chemistry and Physics*, 75th ed.; CRC Press: Boca Raton, 1994.

(52) Singh, H. N.; Saleem, S. M.; Singh, R. P.; Birdi, K. S. Micelle formation of ionic surfactants in polar nonaqueous solvents. *Journal of Physical Chemistry* **1980**, *84*, 2191–2194.

(53) Mitsionis, A. I.; Vaimakis, T. C. Estimation of AOT and SDS CMC in a methanol using conductometry, viscometry and pyrene fluorescence spectroscopy methods. *Chemical Physics Letters* **2012**, *547*, 110–113.

(54) Yaws, C. L.; Richmond, P. C. In *Thermophysical Properties of Chemicals and Hydrocarbons*; Yaws, C. L., Ed.; William Andrew Publishing: Norwich, NY, 2009; Chapter 21, pp 686–781.

(55) Hansen, C. M. *Hansen Solubility Parameters: A Users Handbook*, 2nd ed.; CRC Press: Boca Raton, 2007.

(56) Rüter, A.; Olsson, U. Slow kinetics in a model peptide system. *In preparation*

(57) Rüter, A.; Kuczera, Stefan Stenhammar, J.; Zinn, T.; Narayanan, T.; Olsson, U. Tube to ribbon transition in a self-assembling model peptide system. *In preparation*

(58) Lindner, P., Zemb, T., Eds. *Neutron, X-rays and Light. Scattering Methods Applied to Soft Condensed Matter*, 1st ed.; North Holland: Amsterdam, 2002; p 552.

(59) Koder Hamid, M.; Rüter, A.; Kuczera, S.; Olsson, U. An isothermal titration calorimetry study of peptide self-assembly. *In preparation*

Graphical TOC Entry